Trimeric Plasmonic Molecules: The Role of Symmetry

ARTICLE *in* NANO LETTERS · JUNE 2011

Impact Factor: 13.59 · DOI: 10.1021/nl2008532 · Source: PubMed

2 AUTHORS:

Lev Chuntonov
Weizmann Institute of Science
25 PUBLICATIONS **264** CITATIONS
SEE PROFILE

Gilad Haran
Weizmann Institute of Science
85 PUBLICATIONS **4,037** CITATIONS
SEE PROFILE

THE JOURNAL OF PHYSICAL CHEMISTRY C

ARTICLE

pubs.acs.org/JPCC

Effect of Symmetry Breaking on the Mode Structure of Trimeric Plasmonic Molecules

Lev Chuntonov* and Gilad Haran*

Department of Chemical Physics, Weizmann Institute of Science, Rehovot 76100, Israel

ABSTRACT: Symmetry breaking enriches the spectrum of interactions of surface plasmons with light by introducing phenomena that are not observed in nanostructures with high symmetry. We investigate plasmonic spectra of nanoparticle trimers as a function of a gradual change in their geometry, which implies a smooth transition between different symmetry groups. Three homologous series are presented, starting from an equilateral trimer and ending with either a linear chain of three nanoparticles, a dimer, or a monomer. Degeneracy of the plasmon modes of highly symmetric clusters is lifted, and the energy splitting of the new modes and the corresponding resonance intensities strongly depend on the cluster geometry. Single-cluster optical plasmon spectroscopy is correlated with TEM imaging of the clusters and numerical simulations. The results are understood with the aid of symmetry correlation tables and plasmon-hybridization theory, which reveal the origins of transformations observed in the plasmon spectra. The changes in mode energies and characters that are most crucial for the correct interpretation of mode evolution along the series are found to occur in a narrow range of cluster geometrical parameters, involving in some cases an avoided crossing between two modes.

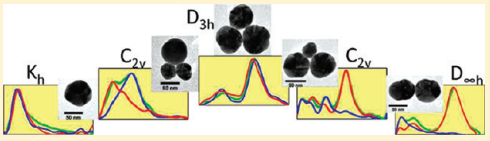

1. INTRODUCTION

Clusters of plasmonic nanoparticles with well-defined geometry have found a broad range of applications, including their use as nanoantennas,[1−3] metamaterials,[4−7] media for amplified emission,[8] and substrates for surface-enhanced Raman,[9−11] surface-enhanced fluorescence[12] and infrared[13] spectroscopy, and as nonbleaching labels for bioimaging.[14,15] Some of these nanostructures have been termed plasmonic molecules (PMs),[16] because their mode structure and optical response resemble the properties of "ordinary" molecules and strongly depend on the symmetry of the nanostructure. Despite numerous recently performed experiments, and significant progress in computational nanoscience, the optical properties of PMs and their relation to phenomena of interest involving the nanoparticles are still not fully understood.[17−19] Numerical simulations are very helpful in the engineering of new nanoscale devices because they help tailoring their optical properties to the specific applications.[10,11,15] However, in many cases, they are not sufficient to provide a desired framework for intuitive understanding of the experimental findings that reflect the nature of interaction between the light and PMs. Therefore, additional investigation is needed to establish a connection between these phenomena and intuitive physical principles, by employing the indicated analogy between plasmonic and standard molecules.

Symmetry breaking (SB) can introduce interactions between plasmon modes that do not interact in PMs with high symmetry and extend the range of their possible applications.[2,4,7,10,15] Among the examples of plasmonic nanostructures in which SB has led to such effects are off-centered nanoshells,[20] nanocavities,[21] nanoparticle dimers,[22,23] and trimers.[24−26] SB can also modify conditions for the appearance of Fano resonances in various plasmonic nanostructures,[27,28] including plasmonic tetramers[29] and higher-order oligomers with various geometries.[30,31] In this work, we study geometric SB in clusters of three silver nanoparticles. We have recently demonstrated how the plasmon modes of trimeric PMs evolve as their vertex angle is gradually opened, using single-cluster optical spectroscopy in correlation with TEM imaging and numerical simulations.[25] We have shown how the degeneracy of the plasmon modes of the symmetric trimer of D_{3h} symmetry is lifted as the trimer gradually transforms to a linear chain of $D_{\infty h}$ symmetry. Invoking plasmon hybridization theory, recently introduced by Nordlander and co-workers,[32] and group correlation tables[33,34] allowed us to follow the plasmon mode evolution and fully understand the mechanisms behind changes observed in the plasmonic spectra, both in the experiments and in numerical simulations. Within the plasmon hybridization approach, collective modes of the cluster of different energies are constructed in a manner analogous to the symmetry-adapted linear combinations of atomic orbitals extensively used in modern chemistry. Therefore, this method provides an intuitive means of exploring plasmonic phenomena. Here we perform a systematic spectroscopic study of trimeric nanoparticle clusters.[24,35,36] Our recently reported observations are extended to additional forms of geometric SB in trimeric PMs. Such a study is a necessary prerequisite for the development of a detailed understanding of light−plasmon interaction in metallic nanostructures with predictive abilities.

This paper is organized as follows. Experimental and theoretical methods are described in section 2. The case of the symmetric trimer is discussed in section 3.1. Plasmon mode evolution is then demonstrated using two different scenarios of SB. The first series, discussed in section 3.2, progresses through a gradual

Received: May 16, 2011
Revised: July 24, 2011
Published: August 19, 2011

decrease in the size of the vertex particle, such that the trimeric cluster gradually transforms into a nanoparticle dimer. The second series, discussed in section 3.3, involves a simultaneous progressive decrease in the size of the base nanoparticles, such that the trimeric cluster gradually transforms into a single nanoparticle, a monomer. Section 3.4 briefly discusses our previous results for the case of SB by vertex angle opening. Altogether, all possible cases of SB in the trimeric PMs with nearly touching nanoparticles are covered in the paper, excluding the cases of clusters without any symmetry elements as, for example, the set of clusters with all three nanoparticles having different sizes. Conclusions and prospects are presented in section 4.

2. METHODOLOGY

Mixtures of aqueous solutions of silver nanoparticles with nominal sizes ranging from 30 to 70 nm (nanoComposix Inc.) were drop-sprayed on the support layer of the carbon-coated TEM grid (200 mesh, EMS). The size of each drop was estimated to be ~500 pL. Solvent evaporation-induced capillary forces stimulated the aggregation of the nanoparticles into clusters. Optical spectra of single clusters were measured with a setup that included an inverted microscope (IX70, Olympus) equipped with a dry dark-field condenser, a variable numerical aperture objective (NA 0.6−1.3), a spectrograph with a back-illuminated CCD (Acton, Princeton), and a 75 W xenon lamp (Olympus). Polarization of the excitation light was controlled by a combination of a polarizer and a selecting sector, such that only s-polarized light reached the sample.[23] TEM imaging (CM120, Philips) was performed immediately after the spectroscopic measurements to prevent possible morphological changes of the clusters because of the oxidation of silver. TEM images and plasmonic spectra of single-nanoparticle clusters were then matched.[37]

Numerical simulations were performed using the Multiple Multipole Program (MMP)[38,39] together with the dielectric function of silver from ref 40, while taking into account also the condensation water present on the nanoparticles in the experiment.[41] All simulations were performed assuming normally incident light. The adequacy of this approach was verified by comparing the experimental spectra with those simulated for other incident angles. This approximation allowed us to utilize the symmetry planes present in the nanoparticle clusters with respect to the polarization of the excitation light, significantly reducing the computational effort. The scattering intensity was calculated by integration of the flux of the time-averaged Pointing vector through an imaginary sphere surrounding the cluster. The interparticle separation was kept at 1 nm in all the simulations, in agreement with TEM images of the nanoparticles taken with the sample tilted in the range of ±40°.

3. RESULTS AND DISCUSSION

3.1. Symmetric Trimer. The plasmon spectra of the symmetric trimer, which takes the form of an equilateral triangle, and the corresponding TEM image are shown in the first row of Figure 1. In particular, in the left panel of Figure 1a, the experimental spectra for excitation with unpolarized light (green lines), light polarized along the base of the trimer (denoted as longitudinal polarization, red lines), and light perpendicular to it (transverse polarization, blue lines) are shown. The black lines on the figure represent the raw experimental data, while the colored lines represent a low-pass filtered version of the data.

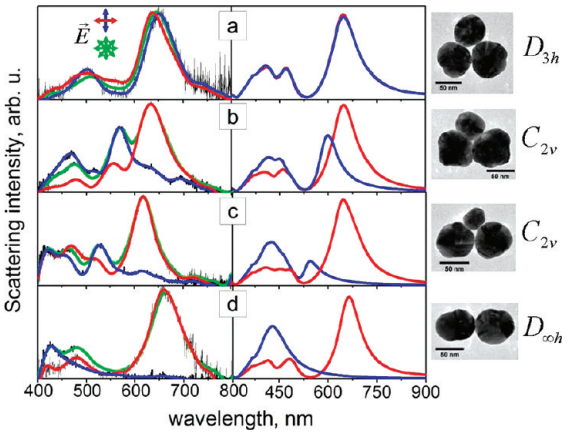

Figure 1. Experimental scattering spectra (left), corresponding TEM images (right; scale bar is 50 nm), and numerical simulations of the plasmon spectra of symmetry-broken trimers for different sizes of the vertex nanoparticle. Green lines denote excitation by the nonpolarized light, red lines excitation by linearly polarized light along the trimer's base, and blue lines excitation by light polarized perpendicularly with respect to the trimer's base. Polarized spectra are normalized to the corresponding peaks of the nonpolarized spectra. The sizes of vertex nanoparticle (R_1) used in the simulations (middle) are 32, 24, 16, and 0 nm, corresponding to R_1/R_2 values of 1, 0.75, 0.5, and 0, respectively. The corresponding symmetry point groups are indicated at the right.

There is good agreement between the experimental results and numerical simulations shown in the middle panel of Figure 1a. To improve our understanding of the physics of the plasmon resonances observed in the spectra, we analyzed the charge distributions induced on the surfaces of the nanoparticles. The charge distributions calculated numerically by the MMP for excitation of the plasmon modes of the symmetric trimer at their resonant wavelengths for both longitudinal and transverse polarizations are shown in Figure 2 (left column).

The symmetric trimer belongs to the D_{3h} symmetry group. Collective plasmon modes of the trimer are constructed from linear combinations of individual nanoparticle plasmon modes, in analogy to molecular orbitals, which are constructed from linear combinations of atomic orbitals. The appearance of the doubly degenerate modes corresponding to the irreducible representations of the E' symmetry is dictated by the presence of the symmetry element corresponding to the 3-fold rotation operation. Linear combinations of degenerate modes can in principle be selected such that the individual nanoparticle plasmon modes will have real coefficients. The two pairs of new modes can be classified as bonding or antibonding, depending on their energy.[24] This work focuses on the collective modes built up by the dipolar modes of the individual nanoparticles. Within this approximation, each pair of the E' cluster modes has one mode with a non-zero total dipole moment in the transverse direction, while the other has its dipole moment in the longitudinal direction. The mode having a non-zero dipole moment in the transverse direction is symmetric with respect to the σ_v reflection plane that is perpendicular to the cluster's base, while the mode having a non-zero dipole moment in the longitudinal direction is antisymmetric. The modes are illustrated in the left column of Figure 3. Note that in this work we address only the in-plane modes of the clusters.

Assignment of the spectral peaks seen in Figure 1 to the plasmon modes shown in Figure 3 is based on the results of the

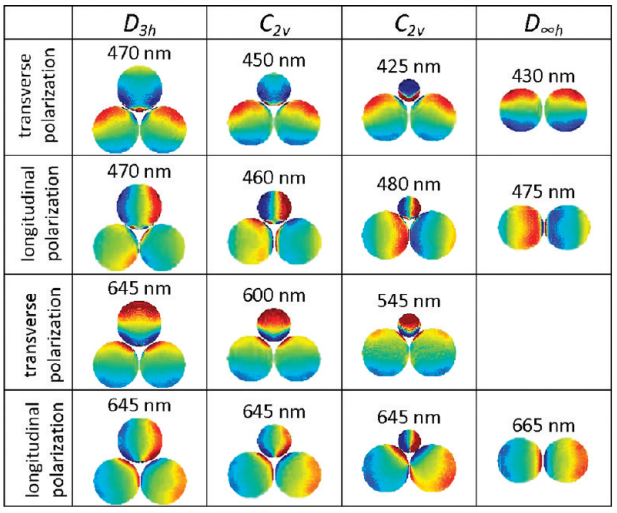

Figure 2. Charge distribution induced on the surface of the nanoparticles calculated numerically with the MMP for the plasmon resonances shown in Figure 1. The corresponding resonance wavelength is indicated in each case.

numerical simulations. The bonding and antibonding E' resonances are assigned to the spectral peaks at 650 and 470 nm, respectively. The contribution of the assigned modes to the charge distribution induced on the surface of the nanoparticles exceeds 50% in all cases. Indeed, the correspondence between the calculated charge distributions (Figure 2) and the dipolar modes shown in Figure 3 is evident by eye. However, additional contributions from modes of higher orders, such as quadrupole, etc., are also present.[24] The degeneracy of the E' modes is reflected in the very similar spectral shape obtained with longitudinal and transverse polarization of the excitation light in both experimental and numerical spectra. The peak that appears at 405 nm in the simulated spectra for both transverse and longitudinal excitations arises from strong coupling to high-order modes. For example, the dark A_1' radial mode, which is the highest-energy dipolar mode of the D_{3h} trimer, mixes with the quadrupole modes. Additional high-order modes can also contribute in this spectral region. The details of this coupling, however, are beyond the scope of this work. The relatively small cross section of the peak at 405 nm in the experimental spectrum as compared to the simulations can be explained by the low detection efficiency of our system in the short wavelength region.

3.2. Symmetry Breaking by Resizing the Vertex Nanoparticle. Reducing the size of the vertex nanoparticle of the trimer breaks the D_{3h} symmetry of the cluster. In the new symmetry point group C_{2v}, the degeneracy of the bonding and antibonding E' modes is lifted. The effect is most pronounced for the bonding modes at 650 nm, where new peaks corresponding to A_1 (transverse) and B_2 (longitudinal) modes appear, as shown in Figure 1b–d. These modes are selectively excited by light of the corresponding polarization, as shown by the blue and red spectra. The corresponding calculated charge distributions at the resonant wavelengths are shown in Figure 2. The experimental results, confirmed by the numerical simulations, show that the transverse bonding mode gradually shifts to the blue and loses its intensity, while the longitudinal bonding mode does not change its position. The antibonding E' modes also split with the breaking of the cluster symmetry. This splitting in the blue region of the spectrum is accompanied by strong mixing of the dipole modes

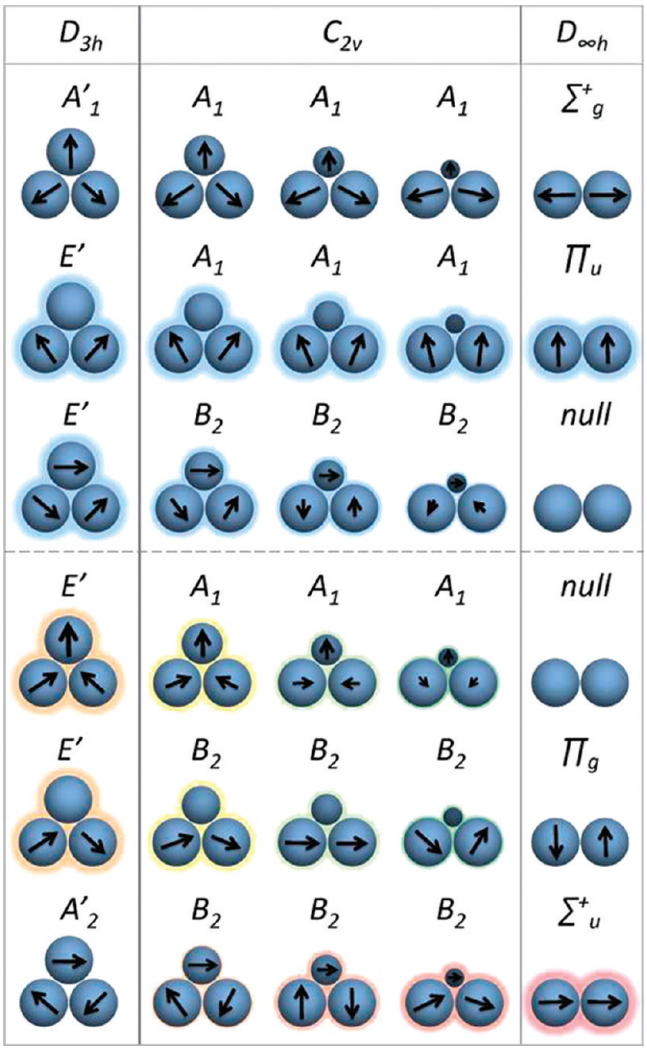

Figure 3. Correlation between dipolar plasmon eigenmodes of trimers for varying sizes of vertex particle R_1, obtained using plasmon hybridization theory. The interparticle separation is 1 nm. The top half shows antibonding modes and the lower half bonding modes. The symbols of the corresponding irreducible representations are shown. The thickness of halos surrounding the particles represents the relative "brightness" of plasmon modes, while their color corresponds approximately to the resonance wavelength.

of the cluster with the higher-order modes. This is especially obvious in panels b and c of Figure 1, where several additional new peaks appear.

Plasmon hybridization theory provides an in-depth understanding of the mechanisms leading to the observed change in the plasmon spectra. We calculated the eigenmodes of the symmetry-broken trimers and their plasmon energies for different sizes of the vertex nanoparticle by solving the corresponding Euler–Lagrange equations for the deformations of the free electron liquid on the surface of the nanoparticle.[32] The optical response of silver was modeled by the Drude dielectric function with $\omega_B = 9.5$ eV, $\varepsilon_S = 5$, and $\varepsilon_E = 1.8$, where ω_B is the bulk plasmon frequency, ε_S is the background polarizability of the metal ions, and ε_E is the permittivity of the medium surrounding the nanoparticles.[24] The eigenmodes are shown schematically in Figure 3, while the dependence of the calculated energies on the vertex nanoparticle size is shown in Figure 4. A detailed

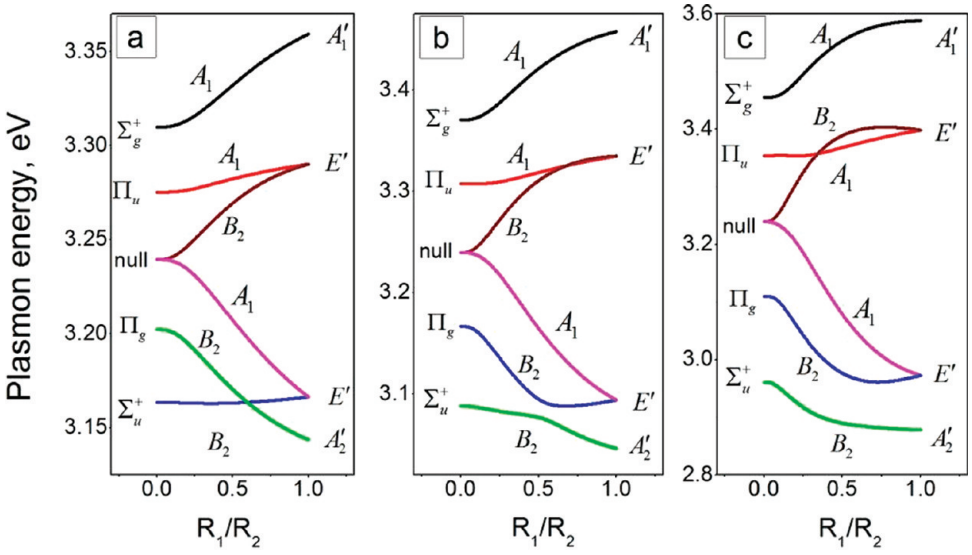

Figure 4. Plasmon energies of the in-plane eigenmodes of symmetry-broken trimers for different ratios of the radii of the vertex particle (R_1) and base particles (R_2 = 32 nm), calculated by plasmon hybridization theory. The interparticle separations are (a) 33, (b) 14, and (c) 1 nm. The model includes only dipolar terms. The symmetry symbols of the plasmon modes are marked in agreement with the symmetry group correlation tables: $R_1/R_2 = 1$ corresponds to D_{3h}, $0 < R_1/R_2 < 1$ corresponds to C_{2v}, and $R_1/R_2 = 0$ corresponds to $D_{\infty h}$.

theoretical description of the charge distributed on the nanoparticle surface by the plasmon hybridization method requires consideration of a full multipole expansion series at the origin of each nanoparticle. Here, for the sake of simplicity, we accounted for only the dipolar ($l = 1$) terms. When the nanoparticles are in the proximity of each other and strongly interact, terms of multipole orders higher than dipolar may admix into the dipolar modes and modify their character. For example, such admixing of the quadrupolar modes into the dark dipolar mode in the nanoparticle dimer makes this mode weakly visible in the plasmon spectrum.[23] However, the energies of the higher-order modes are significantly higher than the energies of the bonding modes of the trimers shown in Figure 1, and therefore, to a first approximation, the former can be omitted in the analysis of the bonding modes. Although the actual eigenvalues obtained by the plasmon hybridization calculation within the dipole limit are higher in energy than the experimental and numerical results of Figure 1, the qualitative trends in the eigenvalue evolution obtained by this simplified approach are preserved. Better agreement with the experimental data is obtained when plasmon modes of up to the $l = 10$ order are considered. However, this significantly complicates the intuitive understanding of the interaction picture.

The diagrams of Figure 4 demonstrate the evolution of the plasmon mode energy as the size of the vertex nanoparticle of radius R_1 is reduced relative to the size of the base nanoparticles that is kept constant and equal to 32 nm (R_2). The plasmon energies are plotted as a function of the R_1/R_2 ratio such that $R_1/R_2 = 1$ corresponds to the D_{3h} cluster, $0 < R_1/R_2 < 1$ to the C_{2v} cluster, and $R_1/R_2 = 0$ to a dimer having $D_{\infty h}$ symmetry. The three panels of the figure show the calculations for different interparticle separations. The calculated energy curves clearly reproduce the splitting of the E' modes of the broken-symmetry clusters as obtained experimentally and with numerical simulations (see Figure 1). The degenerate E' modes are split into two modes: A_1 (transverse) and B_2 (longitudinal). First, we discuss the evolution of the A_1 mode that originates from the transverse E' mode of the D_{3h} symmetry cluster. The energy of the A_1 mode gradually increases with a decrease in R_1, and the total dipole moment of the mode decreases, as schematically illustrated in Figure 3. The A_1 mode eventually transforms to the null mode of the dimer, in which there is no charge induced on the surface of the nanoparticles. This evolution is consistent also with the gradual decrease in the scattering cross section of this mode. The appearance of the null mode is due to the vanishing size of the vertex nanoparticle, such that the dimer having $D_{\infty h}$ symmetry has three fewer degrees of freedom than the trimeric cluster. The energy of the null mode corresponds to the energy of the monomer, as shown in Figure 4, because for this mode in our theoretical modeling all the induced charge amplitude is localized on the vertex nanoparticle with a zero radius, while the amplitude on the base nanoparticles is essentially zero. Therefore, this artificial mode appears in the case of the dimer due to the application of a basis set suitable for a trimer, which has more degrees of freedom.

Next, we discuss the evolution of the longitudinal bonding modes originating from the E' and A_2' bonding modes of the D_{3h} symmetry cluster. Both modes transform into antisymmetric modes of B_2 symmetry. As shown in Figure 4, the details of the plasmon mode evolution depend on the interparticle separation. Energy diagrams for three different interparticle separations are shown: (a) 33, (b) 14, and (c) 1 nm. When the nanoparticles are placed far apart, the interaction between them is weak. In such a case, the energy curves of the same symmetry can cross, as shown for example in Figure 4a, where the curves corresponding to the two bonding B_2 modes originating from the longitudinal E' and A_2' modes of the D_{3h} cluster cross when $R_1/R_2 = 0.6$. Here, the B_2 mode originating from the E' mode transforms to the Σ_u^+ mode of $D_{\infty h}$, while the B_2 mode originating from the A_2' mode transforms to the Π_g mode. Reducing the interparticle separation increases the strength of the interaction between these two B_2 modes, and the corresponding curves now present an avoided crossing, as shown in panels b and c of Figure 4. The smaller the interparticle distance, the stronger the interaction between the nanoparticles and the larger the splitting between the curves.

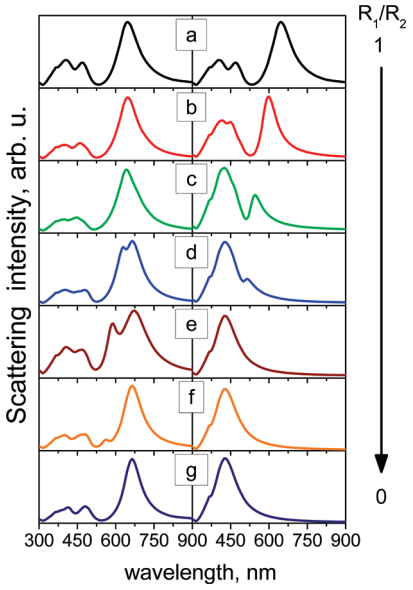

Figure 5. Plasmon scattering spectra obtained from the numerical simulations (MMP) for clusters excited with longitudinal (left) and transverse (right) light polarization for the gradual decrease in the size of the vertex nanoparticle. The sizes of the nanoparticles within the cluster are as follows: $R_2 = 32$ nm, and (a) $R_1 = 32$ nm ($R_1/R_2 = 1$), (b) $R_1 = 24$ nm ($R_1/R_2 = 0.75$), (c) $R_1 = 16$ nm ($R_1/R_2 = 0.5$), (d) $R_1 = 12$ nm ($R_1/R_2 = 0.375$), (e) $R_1 = 8$ nm ($R_1/R_2 = 0.25$), (f) $R_1 = 6$ nm ($R_1/R_2 = 0.1875$), and (g) $R_1 = 0$ nm ($R_1/R_2 = 0$).

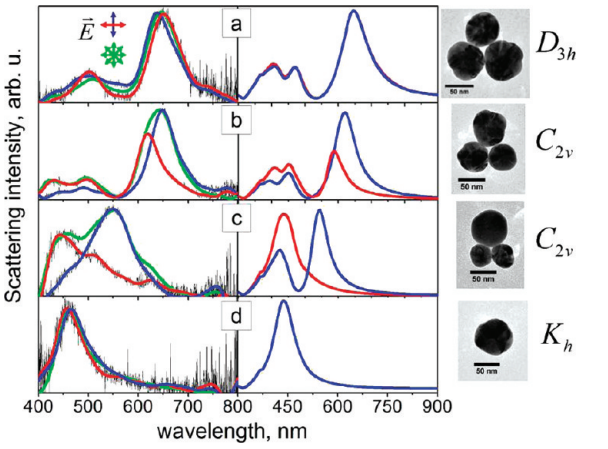

Figure 6. Experimental scattering spectra (left), corresponding TEM images (right; scale bar is 50 nm), and numerical simulations of the plasmon spectra of symmetry-broken trimers for different sizes of base nanoparticles. Green lines represent excitation by the nonpolarized light, red lines excitation by linearly polarized light along the trimer's base, and blue lines excitation by light polarized perpendicularly with respect to the trimer's base. The sizes of the base nanoparticles R_2 used in the simulations (middle) are 32, 24, 8, and 0 nm, corresponding to R_2/R_1 ratios of 1, 0.75, 0.25, and 0, respectively. Polarized spectra are normalized to the corresponding peaks of the nonpolarized spectra. The corresponding symmetry point groups are indicated at the right.

The avoided crossing implies that the evolution of the plasmon modes is different than in the case of a weak interaction, such that the B_2 mode originating from E' transforms to the Π_g mode of $D_{\infty h}$, while the B_2 mode originating from A_2' transforms to the Σ_u^+ mode. While the Σ_u^+ mode is the bright bonding mode of the dimer, the Π_g mode is a dark transverse mode, which is not observed at all in the scattering spectrum.

In summary, in the weak interaction case of Figure 4a, the bright E' mode of D_{3h} transforms to the bright Σ_u^+ mode of $D_{\infty h}$ and the dark A_2' mode transforms to the dark Π_g mode. In the strong interaction case of Figure 4c, the bright E' mode transforms to the dark Π_g mode, while the dark A_2' mode transforms to the bright Σ_u^+ mode. The latter case is directly relevant to our experimental results. Here, the total dipole moment of the B_2 mode originating from E' gradually decreases and that of the B_2 mode originating from A_2' gradually increases, as also seen in Figure 3. The magnitude of the total dipole moments of the two B_2 modes of C_{2v} becomes equal approximately when $R_1/R_2 = 0.35$, and the energy separation between the modes for this ratio is sufficient for them to be, in principle, clearly distinguished in the scattering spectrum. We performed detailed MMP-based numerical simulations that confirmed the spectral shapes predicted by the plasmon hybridization analysis. The corresponding simulated spectra are shown in Figure 5, showing that two longitudinal bonding plasmon resonances can be resolved in the scattering spectrum, however, only in the narrow range of $0.2 < R_1/R_2 < 0.4$. For R_1/R_2 values outside this range, either the total dipole moment magnitude of one of the modes is too low to be observed or the energy separation between the two modes is insufficient.

Antibonding degenerate E' modes also split into A_1 and B_2 modes. Upon the transition from the D_{3h} group to the $D_{\infty h}$ group, the total dipole moment of the longitudinal antibonding B_2 mode decreases and transforms into the null mode of the dimer, while the transverse A_1 mode transforms into the Π_u mode. As shown in Figure 4, for any choice of interparticle distances, these two modes of the C_{2v} group can cross, because they belong to different irreducible representations and, thus, do not interact. The dark radial A_1' mode transforms into the A_1 mode of the C_{2v} group and then to the dark antibonding Σ_g^+ mode of the dimer.

3.3. Symmetry Breaking by Resizing the Base Nanoparticles. Another scenario of SB in plasmonic trimers studied in this work involves a simultaneous gradual change in the size of the two base particles. The corresponding homologous series starts again with the equilateral triangle of D_{3h} symmetry and includes clusters with a decreasing base particle sizes, corresponding to the C_{2v} symmetry group, down to the "cluster" composed of a single particle only, corresponding to the K_h symmetry group. The experimental scattering spectra for such a series are shown in Figure 6 (left column) together with the results of numerical simulations (middle column) and TEM images of the corresponding clusters. As in the series discussed above, resizing of the base nanoparticles results in lifting of the E' mode degeneracy. The mode splitting is best seen in the scattering spectra for bonding modes of the cluster. Indeed, two new bonding modes are selectively excited by light with the proper polarization: a transverse A_1 mode and a longitudinal B_2 mode.

As the size of the base nanoparticles is reduced, both transverse and longitudinal bonding modes are shifted to the blue, toward the plasmon resonance of the monomer at 450 nm, and the intensity of the corresponding peaks decreases relative to the intensity of the antibonding modes. As opposed to the previous case, in which the D_{3h} cluster transforms into a dimer, when the base particles are resized the longitudinal B_2 mode shifts to the blue "faster" than the transverse A_1 mode. This effect is clearly

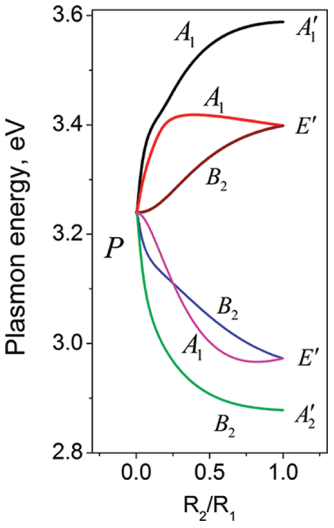

Figure 7. Plasmon energies of the in-plane eigenmodes of symmetry-broken trimers for different ratios of the radii of the base particles R_2 and vertex particle R_1 (32 nm), calculated by plasmon hybridization theory. The interparticle separation is 1 nm. The model includes only dipolar terms. The symmetry symbols of the plasmon modes are marked in agreement with the symmetry group correlation tables: $R_2 = 1$ corresponds to D_{3h}, $0 < R_2/R_1 < 1$ corresponds to C_{2v}, and $R_2/R_1 = 0$ corresponds to K_h.

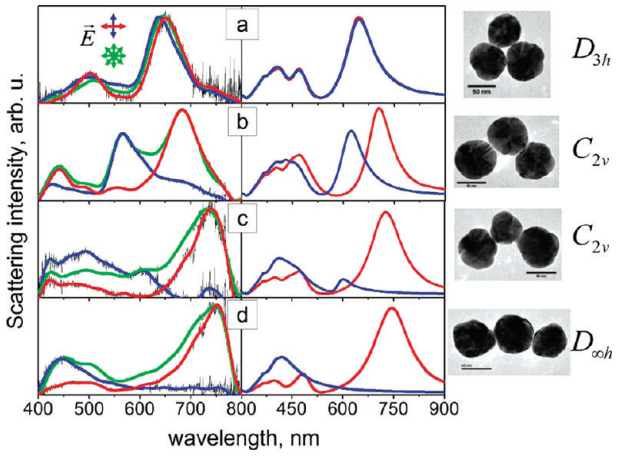

Figure 8. Experimental scattering spectra (left), corresponding TEM images (right; scale bar is 50 nm), and numerical simulations of the plasmon spectra of symmetry-broken trimers for different vertex angles. Green lines represent excitation by nonpolarized light, red lines excitation by linearly polarized light along the trimer's base, and blue lines excitation by light polarized perpendicularly with respect to the trimer's base. Polarized spectra are normalized to the corresponding peaks of the nonpolarized spectra. The values of the vertex angles used in the simulations (middle column) are 60° (a), 90° (b), 140° (c), and 180° (d). The corresponding symmetry point groups are indicated at the right.

seen from a comparison of panels b and c of Figure 6: while the energy of the A_1 mode is still low and the corresponding plasmon resonance peak appears around 500 nm, the longitudinal B_2 mode has already lost its intensity and its energy has converged to the energy of the monomer plasmon. This observation is in agreement with the shapes of the energy curves of the corresponding plasmon states obtained with the plasmon hybridization theory and shown in Figure 7. The curve corresponding to the A_1 mode shows that its energy does not changes significantly when $R_2/R_1 > 0.5$, while the energy of the B_2 mode more rapidly approaches the value of the plasmon resonance of the monomer. Within the paradigm of plasmonic molecules employed in this work, the single particle can be termed a plasmonic atom of K_h symmetry, with its lowest-energy dipolar mode belonging to the P irreducible representation. The P mode is triply degenerate, analogous to the p_x, p_y, and p_z orbitals of real atoms. Here, two of the degenerate modes correspond to the longitudinal and transverse in-plane excitations.

Plasmon hybridization analysis suggests that just as in the case of the homologous series discussed above, the two bonding B_2 modes of the C_{2v} group clusters originating from the E' and A_2' modes of D_{3h} have initially non-zero dipole moments. The dipole moment of the B_2 mode originating from the E' mode of D_{3h} decays, while that of the dark A_2' mode increases with a decrease in the size of the base nanoparticles. The modes reach comparable magnitudes within the narrow R_2/R_1 range of 0.4−0.6. The broadening of the peaks, however, can hinder their explicit spectral separation. During the transition among the D_{3h}, C_{2v}, and K_h symmetry groups, the antibonding modes also converge to the P modes of the monomer. This transition is seen from the corresponding energy diagram shown in Figure 7. Note again that because we account for only the dipolar terms in this model, the energy curves of the antibonding modes serve only as first-order approximations of their exact shape.

3.4. Symmetry Breaking by Opening the Vertex Angle. For the sake of completeness, we briefly repeat here results previously reported in ref 25. The D_{3h} symmetry can also be broken by opening one of the vertex angles (ϕ) of the triangle. The resulting cluster has C_{2v} symmetry for $60 < \varphi < 180$ and $D_{\infty h}$ for $\varphi = 180$. Consequently, SB lifts the degeneracy of the E' modes. As in the previous cases, this effect is best seen for the bonding modes at 650 nm, where we observe new peaks selectively excited by the polarized light. The results are as shown in panels b and c of Figure 8, where the excitation of the A_1 (blue line) and B_2 (red line) modes is demonstrated using transverse and longitudinal light polarization, respectively. As ϕ increases, the plasmon resonance corresponding to the A_1 mode gradually shifts to the blue and its intensity decreases as it is gradually transformed to the Π_u dark transverse mode of the trimeric linear chain having $D_{\infty h}$ symmetry, which is higher in energy than the original E' mode. The longitudinal E' mode of D_{3h} correlates to the B_2 mode of C_{2v} and, with a further increase in ϕ, gradually transforms into another dark mode of the $D_{\infty h}$ cluster, Π_g, which is also higher in energy than the original E' mode. On the other hand, the A_2' dark mode of D_{3h} correlates to a different B_2 mode of C_{2v} and then to a bright longitudinal Σ_u^+ mode of $D_{\infty h}$, which is lower in energy than the original E' mode.

To understand this evolution of the plasmon resonances, we again invoke the plasmon hybridization method. We have shown[25] that a significant evolution of the plasmon modes, which includes a blue shift and the associated decrease in intensity of the first B_2 mode mentioned above, and an increase in the intensity of the second B_2 mode, occurs within a narrow range of vertex angles ($60° < \phi < 80°$). In this region of ϕ, the dipole moments of both B_2 modes are non-zero and the modes can show up in the scattering spectrum. The B_2 mode observed in the scattering spectrum of the clusters with $\phi > 80°$ originates from the A_2' mode of D_{3h}, whereas the B_2 mode originating from E' longitudinal mode of D_{3h} is not observed as its dipole moment is

rather small. Like the cases studied in the previous sections, the transformation that is crucial for the correct understanding of the mode evolution occurs over a narrow range of the geometric parameters of the cluster.

4. CONCLUSIONS

We demonstrated here how the mode structure of trimeric plasmonic molecules is affected by changing their geometry and, consequently, their symmetry. The homologous series of symmetry-broken clusters demonstrated here comprehensively cover all possible configurations of symmetric trimers of nearly touching nanoparticles, excluding those for which all nanoparticles have different sizes and the symmetry operations are not applicable. Each series starts from the equilateral triangle. By gradually reducing the size of one or two nanoparticles, one obtains a cluster that converges to a dimer or a monomer, respectively. On the other hand, gradual opening of the trimer's vertex angle transforms it into a linear chain. The evolution of the plasmon spectra observed experimentally is found to be in a good agreement with the numerical simulations. The results are explained with the help of group correlation tables and plasmon hybridization theory. We have found that changes in mode energies and characters mostly critical for a correct understanding of their evolution occur within a narrow range of geometric parameters and can be easily overlooked. Plasmon hybridization theory is demonstrated to allow for efficient tracing of the mode evolution details.

This work connects the picture of plasmonic eigenmodes of the clusters and the far-field properties of the absorbed and scattered light. A natural extension of this work will be the connection to the near-field properties, which are very important, for example, for single-molecule Raman spectroscopy. In addition, we expect this work to serve as a guide for the design of new devices that will efficiently control light on the nanoscale. In particular, trimeric nanoantennas have recently been shown to rotate the polarization of light,[2] and the directionality of the light scattered by trimers has been recently investigated.[42] Analysis of the experimental and numerical results within the framework of plasmon eigenmodes similar to that presented here can help to improve our understanding of these and similar phenomena by providing an intuitive physical basis.

AUTHOR INFORMATION

Corresponding Author

*E-mail: lev.chuntonov@weizmann.ac.il or gilad.haran@weizmann.ac.il.

ACKNOWLEDGMENT

We acknowledge valuable discussions with Profs. Adi Stern (Weizmann Institute of Science) and Peter Nordlander (Rice University, Houston, TX). This research was made possible by a grant from the Israel Science Foundation (450/10).

REFERENCES

(1) Mühlschlegel, P.; Eisler, H.-J.; Martin, O. J. F.; Hecht, B.; Pohl, D. W. *Science* **2005**, *308* (5728), 1607–1609.

(2) Shegai, T.; Li, Z.; Dadosh, T.; Zhang, Z.; Xu, H.; Haran, G. *Proc. Natl. Acad. Sci. U.S.A.* **2008**, *105* (43), 16448–16453.

(3) Li, Z.; Shegai, T.; Haran, G.; Xu, H. *ACS Nano* **2009**, *3* (3), 637–642.

(4) Fan, J. A.; Wu, C.; Bao, K.; Bao, J.; Bardhan, R.; Halas, N. J.; Manoharan, V. N.; Nordlander, P.; Shvets, G.; Capasso, F. *Science* **2010**, *328* (5982), 1135–1138.

(5) Urzhumov, Y. A.; Shvets, G.; Fan, J. A.; Capasso, F.; Brandl, D.; Nordlander, P. *Opt. Express* **2007**, *15* (21), 14129–14145.

(6) Liu, N.; Langguth, L.; Weiss, T.; Kastel, J.; Fleischhauer, M.; Pfau, T.; Giessen, H. *Nat. Mater.* **2009**, *8* (9), 758–762.

(7) Liu, N.; Giessen, H. *Angew. Chem., Int. Ed.* **2010**, *49* (51), 9838–9852.

(8) Noginov, M. A.; Zhu, G.; Bahoura, M.; Adegoke, J.; Small, C.; Ritzo, B. A.; Drachev, V. P.; Shalaev, V. M. *Appl. Phys. B: Lasers Opt.* **2007**, *86* (3), 455–460.

(9) Michaels, A. M.; Nirmal, M.; Brus, L. E. *J. Am. Chem. Soc.* **1999**, *121*, 9932–9939.

(10) Haran, G. *Acc. Chem. Res.* **2010**, *43* (8), 1135–1143.

(11) Camden, J. P.; Dieringer, J. A.; Zhao, J.; Van Duyne, R. P. *Acc. Chem. Res.* **2008**, *41* (12), 1653–1661.

(12) Lakowicz, J.; Ray, K.; Mustafa Chowdhury, M.; Szmacinski, H.; Fu, Y.; Zhang, J.; Nowaczyk, K. *Analyst* **2008**, *133*, 1308–1346.

(13) Aroca, R. F.; Ross, D. J.; Domingo, C. *Appl. Spectrosc.* **2004**, *58* (11), 324A–338A.

(14) Jiang, Y.; Horimoto, N. N.; Imura, K.; Okamoto, H.; Matsui, K.; Shigemoto, R. *Adv. Mater.* **2009**, *21* (22), 2309–2313.

(15) Romo-Herrera, J. M.; Alvarez-Puebla, R. A.; Liz-Marzan, L. M. *Nanoscale* **2011**, *3*, 1304–1315.

(16) Wang, H.; Brandl, D. W.; Nordlander, P.; Halas, N. J. *Acc. Chem. Res.* **2007**, *40*, 53–62.

(17) Hoffmann, J.; Hafner, C.; Leidenberger, P.; Hesselbarth, J.; Burger, S. *Proc. SPIE* **2009**, *7390*, 73900J–73900J-11.

(18) Barnes, W. L. *J. Opt. A: Pure Appl. Opt.* **2009**, *11* (11), 114002-1–114002-9.

(19) Kelly, K. L.; Coronado, E.; Zhao, L. L.; Schatz, G. C. *J. Phys. Chem. B* **2003**, *107*, 668–677.

(20) Wang, H.; Wu, Y.; Lassiter, B.; Nehl, C. L.; Hafner, J. H.; Nordlander, P.; Halas, N. J. *Proc. Natl. Acad. Sci. U.S.A.* **2006**, *103* (29), 10856–10860.

(21) Hao, F.; Sonnefraud, Y.; Dorpe, P. V.; Maier, S. A.; Halas, N. J.; Nordlander, P. *Nano Lett.* **2008**, *8* (11), 3983–3988.

(22) Nordlander, P.; Oubre, C.; Prodan, E.; Li, K.; Stockman, M. I. *Nano Lett.* **2004**, *4* (5), 899–903.

(23) Brown, L. V.; Sobhani, H.; Lassiter, J. B.; Nordlander, P.; Halas, N. J. *ACS Nano* **2010**, *4* (2), 819–832.

(24) Brandl, D. W.; Mirin, N. A.; Nordlander, P. *J. Phys. Chem. B* **2006**, *110* (25), 12302–12310.

(25) Chuntonov, L.; Haran, G. *Nano Lett.* **2011**, *11*, 2440–2445.

(26) Yan, B.; Boriskina, S. V.; Reinhard, B. M. *J. Phys. Chem. C* **2011**, *115*, 4578–4583.

(27) Luk'yanchuk, B.; Zheludev, N. I.; Maier, S. A.; Halas, N. J.; Nordlander, P.; Giessen, H.; Chong, C. T. *Nat. Mater.* **2010**, *9* (9), 707–715.

(28) Mukherjee, S.; Sobhani, H.; Lassiter, J. B.; Bardhan, R.; Nordlander, P.; Halas, N. J. *Nano Lett.* **2010**, *10*, 2694–2701.

(29) Fan, J. A.; Bao, K.; Wu, C.; Bao, J.; Bardhan, R.; Halas, N. J.; Manoharan, V. N.; Shvets, G.; Nordlander, P.; Capasso, F. *Nano Lett.* **2010**, *10* (11), 4680–4685.

(30) Lassiter, J. B.; Sobhani, H.; Fan, J. A.; Kundu, J.; Capasso, F.; Nordlander, P.; Halas, N. J. *Nano Lett.* **2010**, *10* (8), 3184–3189.

(31) Hentschel, M.; Saliba, M.; Vogelgesang, R.; Giessen, H.; Alivisatos, A. P.; Liu, N. *Nano Lett.* **2010**, *10*, 2721–2726.

(32) Prodan, E.; Radloff, C.; Halas, N. J.; Nordlander, P. *Science* **2003**, *302*, 419–422.

(33) Wilson, E. B.; Decius, J. C.; Cross, P. C. *Molecular vibrations*; Dover: New York, 1955.

(34) Bunker, P.; Jensen, P. *Molecular Symmetry and Spectroscopy*; NRC Press: Ottawa, ON, 1998.

(35) Alegret, J.; Rindzevicius, T.; Pakizeh, T.; Alaverdyan, Y.; Gunnarsson, L.; Kall, M. *J. Phys. Chem. C* **2008**, *112*, 14313–14317.

(36) Klimov, V.; Guo, G.-Y. *J. Phys. Chem. C* **2010**, *114*, 22398–22405.

(37) Mock, J. J.; Barbic, M.; Smith, D. R.; Schultz, D. A.; Schultz, S. *J. Chem. Phys.* **2002**, *116*, 6755–6759.
(38) Hafner, C. *Phys. Status Solidi B* **2007**, *244* (10), 3435–3447.
(39) Sannomiya, T.; Hafner, C. *J. Comput. Theor. Nanosci.* **2010**, *7* (8), 1587–1595.
(40) Linch, D. W.; Hunter, W. R. In Comments on the optical constants of metals. In *Handbook of optical constants of solids*; Palik, E. D., Ed.; Academic Press: San Diego, 1998.
(41) Mock, J. J.; Smith, D. R.; Schultz, S. *Nano Lett.* **2003**, *3*, 485–491.
(42) Shegai, T.; Brian, B. r.; Miljković, V. D.; Käll, M. *ACS Nano* **2011**, *5* (3), 2036–2041.